

Naval Research Laboratory

Washington, DC 20375-5000



NRL Report 9229

**Multibeam Radar Altimetry: Spaceborne Feasibility
and Airborne Experimentation**

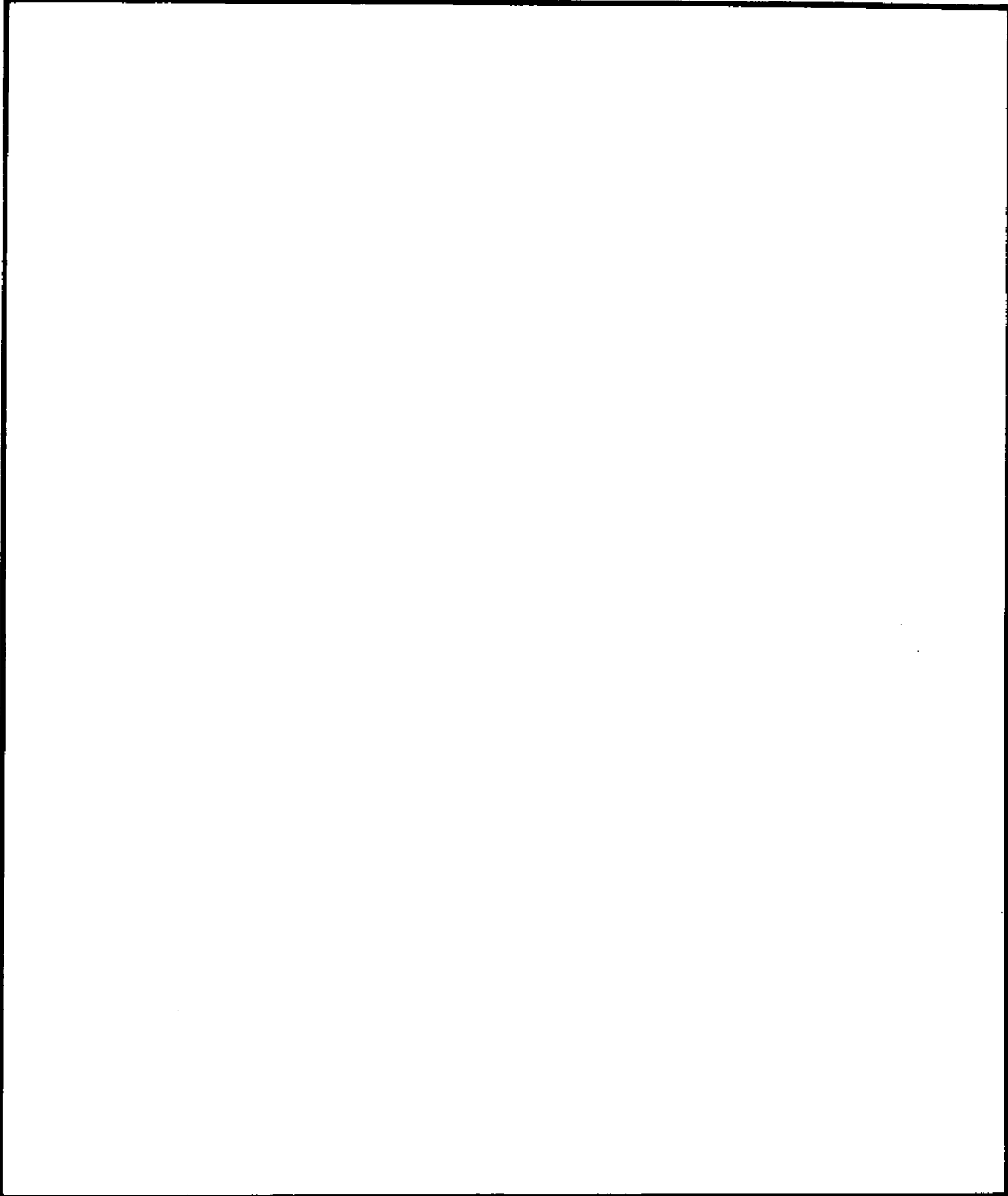
G. S. BROWN, L. S. MILLER, AND L. W. CHOY

*Space Sensing Branch
Space Systems Technology Department*

October 19, 1989

REPORT DOCUMENTATION PAGE				Form Approved OMB No. 0704-0188	
1a. REPORT SECURITY CLASSIFICATION UNCLASSIFIED			1b. RESTRICTIVE MARKINGS		
2a. SECURITY CLASSIFICATION AUTHORITY			3. DISTRIBUTION / AVAILABILITY OF REPORT		
2b. DECLASSIFICATION / DOWNGRADING SCHEDULE			Approved for public release; distribution unlimited.		
4. PERFORMING ORGANIZATION REPORT NUMBER(S) NRL Report 9229			5. MONITORING ORGANIZATION REPORT NUMBER(S)		
6a. NAME OF PERFORMING ORGANIZATION Naval Research Laboratory		6b. OFFICE SYMBOL (If applicable)	7a. NAME OF MONITORING ORGANIZATION		
6c. ADDRESS (City, State, and ZIP Code) Washington, DC 20375-5000			7b. ADDRESS (City, State, and ZIP Code)		
8a. NAME OF FUNDING / SPONSORING ORGANIZATION Space and Naval Warfare Systems Command		8b. OFFICE SYMBOL (If applicable)	9. PROCUREMENT INSTRUMENT IDENTIFICATION NUMBER		
8c. ADDRESS (City, State, and ZIP Code) Washington, DC 20363-5100			10. SOURCE OF FUNDING NUMBERS		WORK UNIT ACCESSION NO.
			PROGRAM ELEMENT NO.	PROJECT NO.	TASK NO.
			63207N	1596	DN680-370
11. TITLE (Include Security Classification) Multibeam Radar Altimetry: Spaceborne Feasibility and Airborne Experimentation					
12. PERSONAL AUTHOR(S) Brown, G. S., Miller, L. S., and Choy, L. W.					
13a. TYPE OF REPORT Final report		13b. TIME COVERED FROM 10/88 TO 5/89		14. DATE OF REPORT (Year, Month, Day) 1989 October 19	15. PAGE COUNT 32
16. SUPPLEMENTARY NOTATION					
17. COSATI CODES			18. SUBJECT TERMS (Continue on reverse if necessary and identify by block number)		
FIELD	GROUP	SUB-GROUP			
			Radar altimetry Multibeam altimetry		
			Space remote sensing		
19. ABSTRACT (Continue on reverse if necessary and identify by block number)					
<p>This report summarizes the results of an investigation into the technical feasibility of multibeam altimetry. Three candidate sensor concepts are considered: a real-aperture system with an approximate 4.5-m antenna for operation at 13.5 GHz or a 1.8-m antenna for operation at 36 GHz; a 13.5 GHz interferometer system; and a 13.5 GHz synthetic aperture system. The overall findings show a preference for the real-aperture system, with a trade-off between the larger antenna required at 13.5 GHz and rain attenuation effects at 36 GHz. Both systems are shown to be capable of providing ≤ 5 cm height resolution and an ≈ 19 km along-track spatial-wavelength resolution for the beam that is pointed 50 km off-nadir in the cross-track direction. An experimental aircraft program is also discussed. The objective is to provide experimental verification of these theoretical findings.</p>					
20. DISTRIBUTION / AVAILABILITY OF ABSTRACT <input checked="" type="checkbox"/> UNCLASSIFIED/UNLIMITED <input type="checkbox"/> SAME AS RPT. <input type="checkbox"/> DTIC USERS			21. ABSTRACT SECURITY CLASSIFICATION UNCLASSIFIED		
22a. NAME OF RESPONSIBLE INDIVIDUAL Lawrence W. Choy			22b. TELEPHONE (Include Area Code) (202) 767-2778	22c. OFFICE SYMBOL Code 8315	

SECURITY CLASSIFICATION OF THIS PAGE



CONTENTS

INTRODUCTION	1
SPACEBORNE FEASIBILITY	3
CANDIDATE SYSTEMS	6
Pure Multiple-Beam System	6
Interferometric Approach	6
Synthetic Aperture Radar Approach	6
PERFORMANCE EVALUATION	7
Pure Multiple-Beam System	7
Interferometric Approach	20
Pseudo SAR	24
Pointing Angle Considerations	25
CONCLUSIONS	25
SUPPORTING AIRCRAFT EXPERIMENTATION	26
ACKNOWLEDGMENTS	27
REFERENCES	27



MULTIBEAM RADAR ALTIMETRY: SPACEBORNE FEASIBILITY AND AIRBORNE EXPERIMENTATION

INTRODUCTION

The U.S. Navy has a high-priority need for an eddy-resolving global ocean prediction system [1] to support antisubmarine warfare (ASW) and other naval operations. This system [2-4] should contain an adequately sampled satellite data input, global surface-wind and heat-flux inputs from atmospheric models, a large computer with a sustained speed of gigaflops and 100 million words of memory, and efficient and validated ocean models for data assimilation and forecasting.

As demonstrated by GEOSAT [5], one can infer subsurface oceanographic parameters with dynamic heights measured by the altimeter. This potential to measure dynamic heights and an all-weather capability make an altimeter the most promising source of global input data for future eddy-resolving global ocean prediction systems [2]. The main drawback of present-day satellite altimetry is that only subsatellite, or line, mapping is furnished. To provide adequate spatial and temporal coverage, a single multibeam altimeter or a multisatellite system with single-beam altimeters is needed.

From the ASW and acoustic modeling point of view [6], the most tactically significant eddies are those with diameters that exceed 100 km. The typical surface swirl velocity of these mesoscale features is in the 10 cm/s to 1 m/s range. To estimate the precision and beam configuration that a multibeam altimeter should have, the geostrophic assumption can be used to compute the sea surface height anomaly Δh that would be generated by the eddies in the open ocean. If C is the swirl velocity, D is the diameter of a circular eddy, g is the acceleration due to gravity, ϕ is the geographic latitude, and Ω is the angular velocity of the earth, the geostrophic analysis gives

$$\Delta h \approx \frac{\Omega \sin \phi}{g} CD.$$

Figure 1 plots this relation. It shows that an altimeter with a height measurement precision of 5 cm could detect eddies whose velocity and diameter combination fall into the area to the right of the $\Delta h = 5$ cm curve at the three indicated latitudes. A precision of ≤ 5 cm is required to detect the most tactically significant eddies.

Figure 2 shows the type of coverage a three-beam altimeter has when the beam spot separation on the sea surface is 50 km. The orbit shown is for an 800-km altitude GEOSAT-type mission with a 17-day exact-repeat track pattern. The solid lines denote the coverage if only a single nadir beam is used. The dotted lines denote the off-nadir beams. The background in Fig. 2 is a phytoplankton pigment image produced by the Coastal Zone Color Scanner aboard NASA's NIMBUS-7 (shown here in black). A warm core eddy is the circular feature in the lower left of the figure.

BROWN, MILLER, AND CHOY

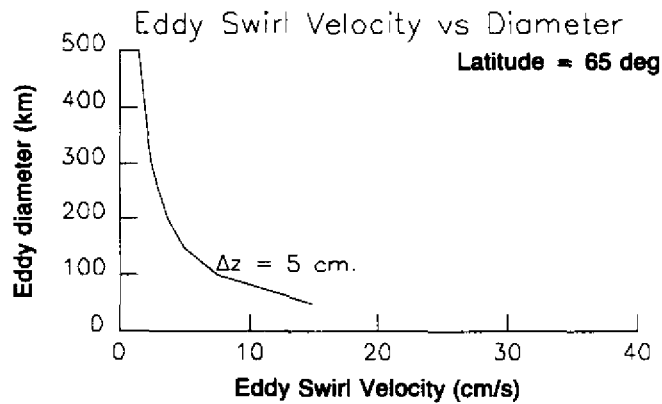
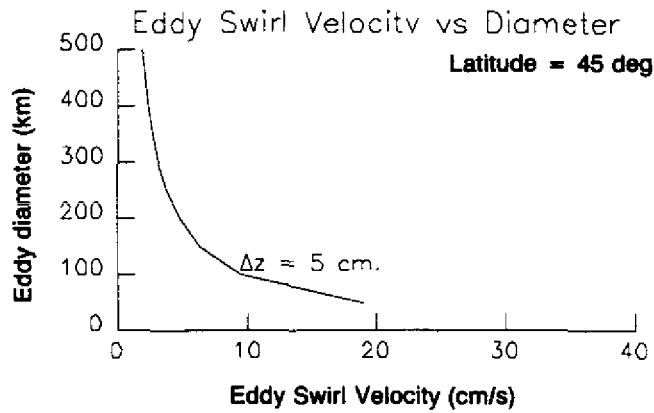
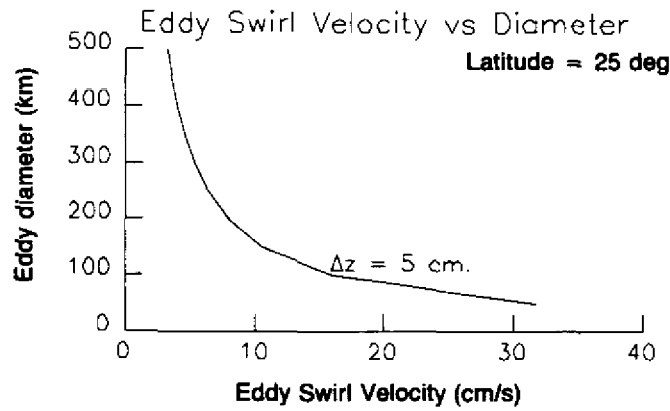


Fig. 1 — An altimeter with a high measurement precision (Δh) > 5 cm could detect eddies whose velocity and diameter combinations fall into the area to the right of the curve at three representative latitudes

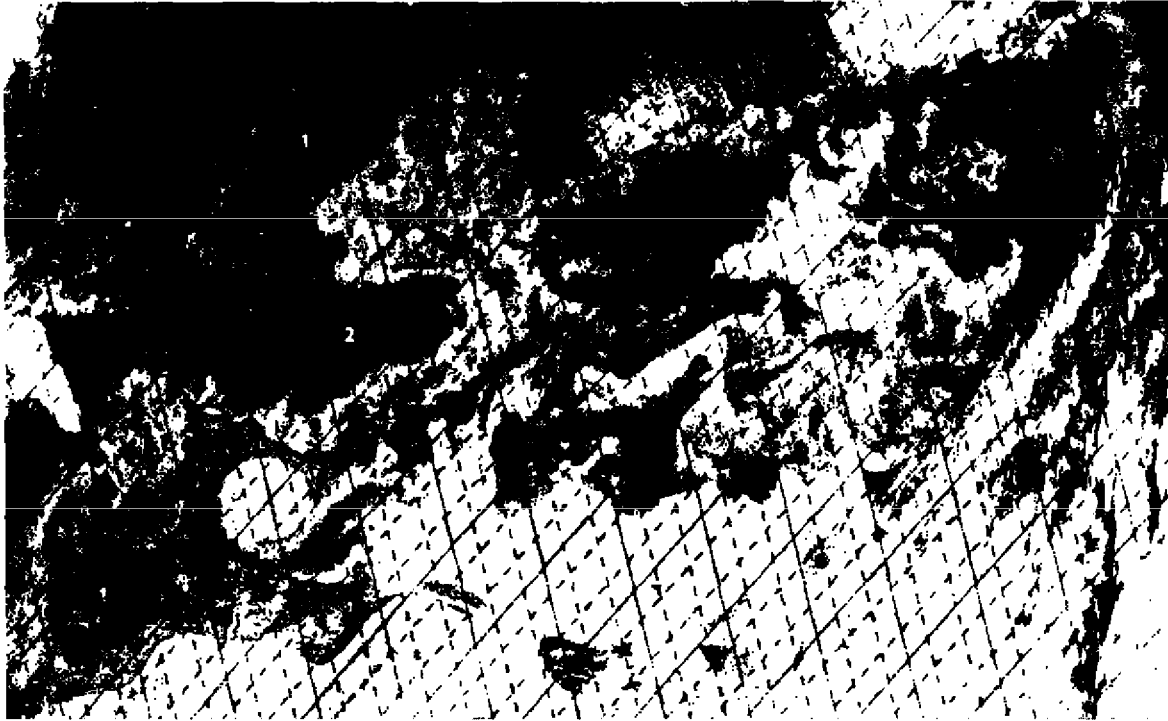


Fig. 2 — The orbit tracks are for an 800-km altitude GEOSAT-type orbit with a 17-day exact-repeat track pattern. The solid lines denote the coverage if only a single nadir beam is used. The dotted lines denote two off-nadir beams. The beam spot separation on the equator is 50 km.

From a measurement point of view, a single altimeter having three beams and 5-cm precision or three satellites each with a single 5-cm precision altimeter are possible configurations. From a multi-beam altimeter system design point of view, a number of questions exist regarding the viability of the multibeam approach. Salient among these are the inherent height and spatial resolution achievable with realistic systems and the pointing angle accuracy. This report focuses on these and other unresolved areas.

We consider only the problem of mesoscale mapping with a beam ground track separation of 50 km. Figure 3 shows the typical geometry. The next section of this report first identifies potential system configurations for accomplishing off-nadir altimetry and then presents a quantitative analysis of the candidate systems. The final section discusses aircraft experiments that are recommended to provide experimental corroboration between NASA/Wallops and the Naval Research Laboratory.

SPACEBORNE FEASIBILITY

In conventional nadir-oriented radar altimetry, the leading edge or ramp portion of the average backscattered return is proportional in its length to the width of the transmitted pulse. The trailing edge of the return is determined primarily by the antenna pattern and, to a lesser degree, the scattering cross section of the surface [7]. The ocean surface waveheight is measured by elongating or

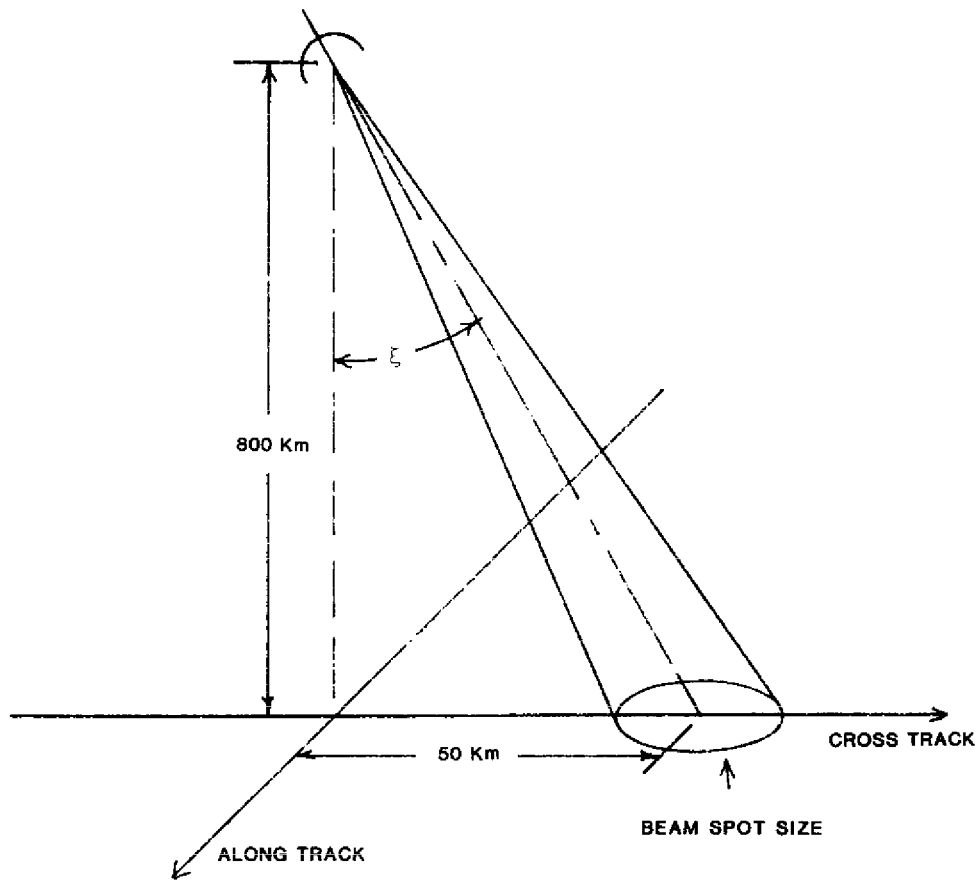


Fig. 3 — Geometry for maximum cross-track beam

stretching the leading edge of the average return. The altitude measurement is also dependent on the shape of the average return. Figure 4(a) shows an average return waveform for a conventional nadir altimeter operating over the ocean; Fig. 4(b) shows a typical off-nadir return.

When an altimeter beam moves off-nadir, the influence of the waveheight and the transmitted pulse shape on the mean return waveform is diminished. In fact, when the off-nadir angle exceeds a very few beamwidths, the shape of the averaged waveforms is almost exclusively determined by the antenna beamwidth [8]. In this case, the average waveform shape is essentially independent of the ocean waveheight. Hence, measuring waveheight does not appear to be possible for off-nadir radar beams. However, the possibility still exists to measure the range to the center of the off-nadir beam and the power backscattered to the radar from this area on the surface. These two measurements hold the promise of both wide swath topographic profiling and wind speed measurement.

The above discussion is intended to define those quantities that can be measured from an off-nadir attitude and those that are measurable but with degraded precision. For these latter quantities, the feasibility of measuring these quantities is directly related to precision. Consequently, the remainder of this report is devoted to estimating the precision with which a given technique can measure the range from the altimeter to the surface by using off-nadir pointed beams. The question

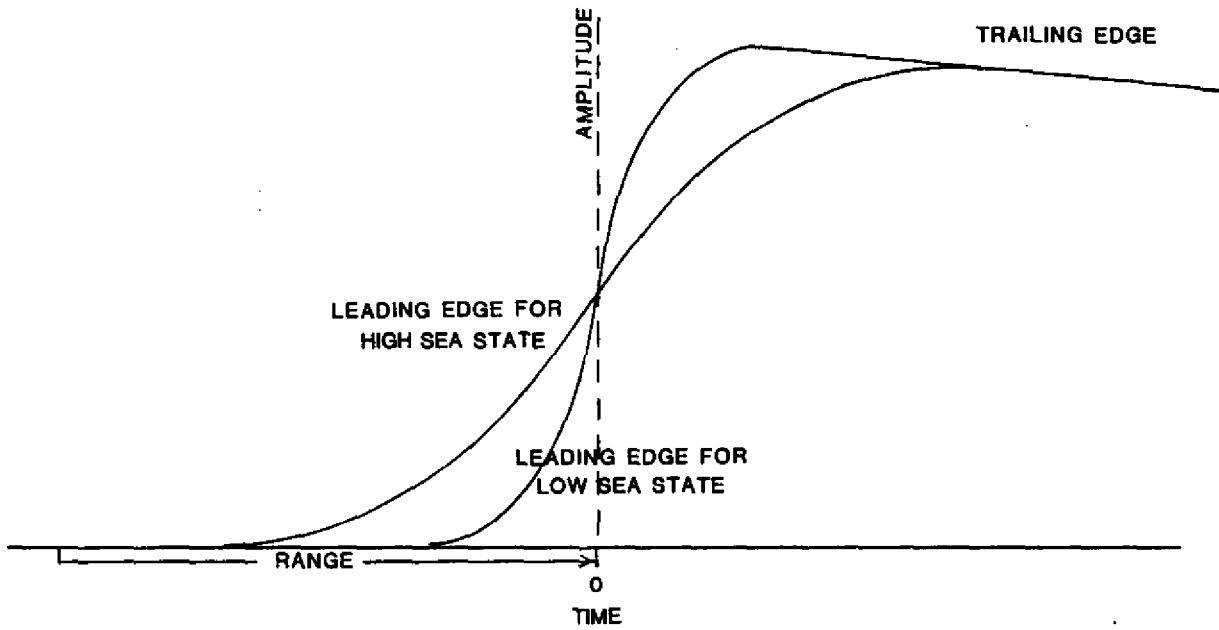


Fig. 4a -- Average return waveform for a conventional nadir altimeter operating over the ocean

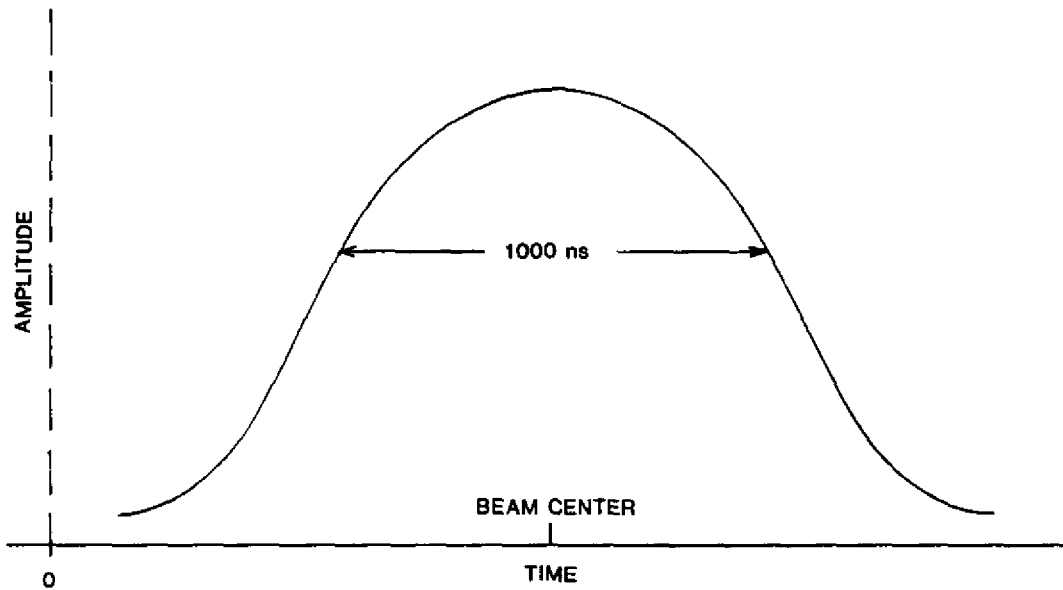


Fig. 4b -- Typical off nadir return plot

of the radar cross section measurement is not directly addressed here because this measurement is inherently much less difficult. That is, the range, or altitude measurement, is significantly more complicated than the return power measurement.

CANDIDATE SYSTEMS

This section describes proposed means for accomplishing wide swath, or off-nadir, altimetry. Subsequent sections consider the precision of these techniques.

Pure Multiple Beam

Brown [9] was the first to propose multiple-beam altimetry to measure cross-track surface slope. This system used a five-beam configuration comprising a nadir directed beam, right- and left-of-track (cross-track) beams, and fore- and aft-pointed (along-track) beams. The two cross-track beams and the nadir beam measured the cross-track slope, and the fore- and aft-pointed beams, in conjunction with the nadir beam, measured along track. The along-track measurement could be compared with the continuous recording by the nadir beam to estimate the precision of the three-beam scheme and to provide precursor information.

Brown [9] did not estimate the precision of this slope-measuring scheme. Since the off-nadir beams pointing angles were restricted to no more than eight beamwidths, the antenna for this system was an offset-fed parabola. For very large antennas, the pointing error was recognized as a potential problem, but using the nadir beam to aid in the attitude determination was considered a practical solution. This system is called a pure multiple-beam system because it uses one independent beam per measurement cell. Of all the systems discussed, this is the most straightforward in concept and easiest to implement.

Interferometric Approach

A drawback of the proposed pure multiple-beam system is that it relies on very narrow beams to achieve the off-nadir topographic measurements. Bush et al. [10] proposed the use of a two-element interferometer to develop very narrow beams along with phasing the elements to shift the beams off nadir. In this approach, the width of the lobes in the interferometer radiation pattern is determined by the spacing between the two antenna elements of the array. The pattern of each element attenuates the array lobes adjacent to the desired lobe. McGoogan and Walsh [11] considered the two-element interferometer to be more suitable for space application than the pure multiple-beam system. In 1985, the Applied Physics Laboratory of Johns Hopkins University [12] developed a conceptual design of an interferometric system for spaceborne applications. This system used two 1.5-m parabolic reflectors displaced by 5 m left of track and 5 m right of track for a total interferometer baseline distance of 10 m. With a 50-km one-sided beam squint, the precision of the resulting range measurement was predicted to be 5 cm with a 5 kHz pulse repetition frequency (PRF).

Synthetic Aperture Radar Approach

Two categories of synthetic aperture radar (SAR) are available for use with global oceanographic altimetry. First, in its simplest implementation, a real aperture can provide cross-track resolution and a synthetic aperture (or Doppler beam sharpening [13]) can provide along-track resolution [14]. With this approach, a narrow rectangular, or fan-beam, antenna would be used. In fact, a

quasi-optics antenna would be required, since a traveling-wave antenna would radiate incrementally as the short pulse (≈ 2 ns) propagated along the aperture.

In the second SAR category, the Naval Research Laboratory (NRL) and others [14,15] have investigated the use of SAR systems within an interferometer configuration. In principle, this technique can provide contiguous cross-track altimetry information. However, questions exist relative to the achievable height accuracy and total system cost and complexity. These and other problem areas are discussed later.

PERFORMANCE EVALUATION

Each of the above systems has features that are attractive either from an implementation or a system perspective. However, these qualities are meaningless unless the design can provide the required topographic precision with the off-nadir beam. This section develops a detailed analysis of the potential performance of each of these systems. The baseline parameters for this evaluation are

- Altitude: $h = 800$ km
- One-sided beam offset: 50 km
- Equivalent pointing angle: $\xi = 3.58^\circ$
- Frequency: 13.5 or 35 GHz
- Antenna aperture efficiency: 56%

A 56% aperture efficiency is somewhat conservative, but it ensures that the results are realistic rather than optimistic. Note that only the outermost beam position is considered, since all of the systems in this study achieve their lowest precision at this outer beam position.

Pure Multiple-Beam System

A key parameter in estimating the precision of this system is the shape of the average return waveform. This waveform is the convolution of three functions: the flat-surface impulse response, the system point target response, and the probability density function of the surface roughness. When the flat-surface impulse response is offset from nadir (as in the case of offset beams) and its time spread (width) is considerably larger than that of the other two functions, the convolution reduces to the product of the flat-surface impulse response and the combined width of the other two functions. When the system point target response and the surface roughness are both Gaussian shaped, the combined width is the root sum square of the widths of each of the individual functions. Combining this result with the asymptotic form for the flat-surface impulse response yields [8]

$$P_r(\tau) = \frac{\eta P_T G_0^2 \lambda^2 \sigma^0(\psi)(cT_c/2)}{(4\pi)^3 L_p r^3} \left[\frac{2\pi}{a(1 + 2b/a)} \right]^{1/2} \exp \left[\frac{-4}{\gamma(1 + \epsilon^2)} [\sin \xi - \epsilon \cos \xi]^2 \right] \quad (1)$$

where

- P_r is received power,
- η is pulse compression ratio,
- P_T is peak transmitted power,
- G_0 is peak boresight antenna gain,
- λ is radar wavelength,
- $\sigma^0(\psi)$ is surface cross section per unit scattering area at the angle ψ
and $\tan \psi = (c\tau/h)^{1/2}$,

- L_p is propagation loss,
 θ_B is antenna half-power beamwidth,
 ξ is angle between the antenna boresight and nadir,
 T_c is composite width (time spread) of the system point target response and the PDF of the surface roughness,
 h is altitude,
 c is speed of light,
 $\epsilon \approx (c\tau/h)^{1/2}$,
 $\tau = t - 2h/c$ ($t = 0$ corresponds to the time when the pulse is transmitted by the radar),
 $\gamma = 2.9 \sin 2(\theta_B/2)$,
 $a = \frac{4 \epsilon \sin 2\xi}{\gamma (1 + \epsilon^2)}$,
 $b = \frac{4 \epsilon^2 \sin 2\xi}{\gamma (1 + \epsilon^2)}$, and
 $r = h(1 + \epsilon^2)^{1/2}$.

This waveform is very nearly Gaussian shaped, as it should be, because the antenna pattern is assumed to be Gaussian. The peak of the return power waveform occurs where

$$\tau_0 = \frac{h}{c} \tan^2 \xi,$$

and for the parameters given previously,

$$\tau_0 \approx 10.44 \mu\text{s}.$$

This is the time of occurrence of the peak in the mean or average return and corresponds to the beam pointing 50 km to one side of nadir. The shape of the return is critical in designing the type of range tracker used to lock-on to and follow this mean return. The design of one type of tracker is discussed next; however, before dealing with the tracker design, it is convenient to derive the time expanse of the waveform given by Eq. (1).

First, ϵ and τ are centered on the peak of the return waveform, i.e.,

$$\epsilon = \epsilon_0 + \delta\epsilon, \quad \tau = \tau_0 + \delta\tau, \quad (2)$$

and $\epsilon_0 = (c\tau_0/h)^{1/2}$. Because $\epsilon = (c\tau/h)^{1/2}$ and $\delta\tau/\tau_0 \ll 1$,

$$\epsilon_0 + \delta\epsilon \approx \left(\frac{c\tau_0}{h} \right)^{1/2} \left[1 + \frac{1}{2} \frac{\delta\tau}{\tau_0} \right] \quad (3)$$

or

$$\delta\epsilon = \frac{1}{2} \delta\tau \left(\frac{c}{h\tau_0} \right)^{1/2}. \quad (4)$$

Substituting these results into the exponential part of Eq. (1) yields

$$\exp \left[\frac{-4}{\gamma(1 + \epsilon^2)} [\sin \xi - \epsilon \cos \xi]^2 \right] \approx \exp \left[-\frac{4}{\gamma} \frac{\cos^2 \xi}{4} \left[\frac{c}{r_0 h} \right] (\delta\tau)^2 \right]. \quad (5)$$

The value of $\delta\tau$ that causes this exponential function to fall to one-half its value at $\delta\tau = 0$ is

$$-\ln(0.5) \left[\frac{h^2 \gamma}{c^2} \right] \left[\frac{\sin^2 \xi}{\cos^6 \xi} \right] = (\delta\tau)^2.$$

The total half-power width is $2\delta\tau$ or

$$2\delta\tau = \frac{2h}{c} \tan \xi [-\gamma \ln(0.5)/\cos^4 \xi]^{1/2}. \quad (6)$$

Substituting from the relationship between γ and the half-power beamwidth yields

$$2\delta\tau = \frac{2h}{c} \frac{\tan \xi}{\cos^2 \xi} \sin(\theta_B/2) (1.42) \quad (7)$$

By using the small angle approximations for both ξ and θ_B , i.e.,

$$\sin(\theta_B/2) \approx \theta_B/2,$$

$$\tan \xi \approx \xi,$$

$$\cos \xi \approx 1,$$

and noting that for a 56% efficient circular aperture [16],

$$\theta_B \approx 1.47\lambda/D, \quad (8)$$

where D is the diameter of the aperture, Eq. (7) becomes

$$2\delta\tau \approx 2.08 \frac{h\xi}{Df}, \quad (9)$$

where f is the frequency of the radar. The corresponding time spread T_e between the e^{-1} values is $T_e = 2.5 (h\xi/Df)$. Figure 5 is a plot the half-power width for the present case. Equation (9) shows that the width of the average return is directly proportional to the altitude and pointing angle of the radar's antenna and is inversely proportional to the antenna aperture diameter and the radar's frequency. Having both the average return's shape and width, an expression can be derived for the error involved in making a waveform-based measurement of the off-nadir range. Figure 6 shows a model receiver system for computing the rms height error.

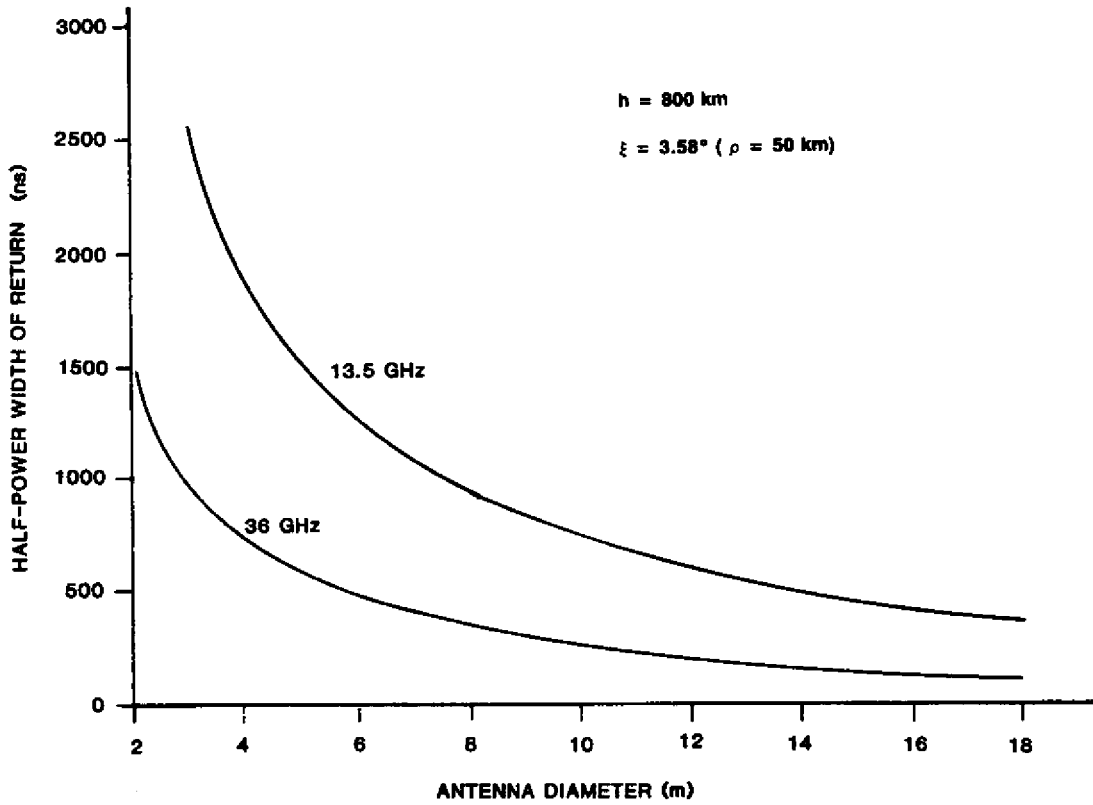


Fig. 5 — Plot of the half-power width of the average return power waveform for a 56% efficient aperture antenna

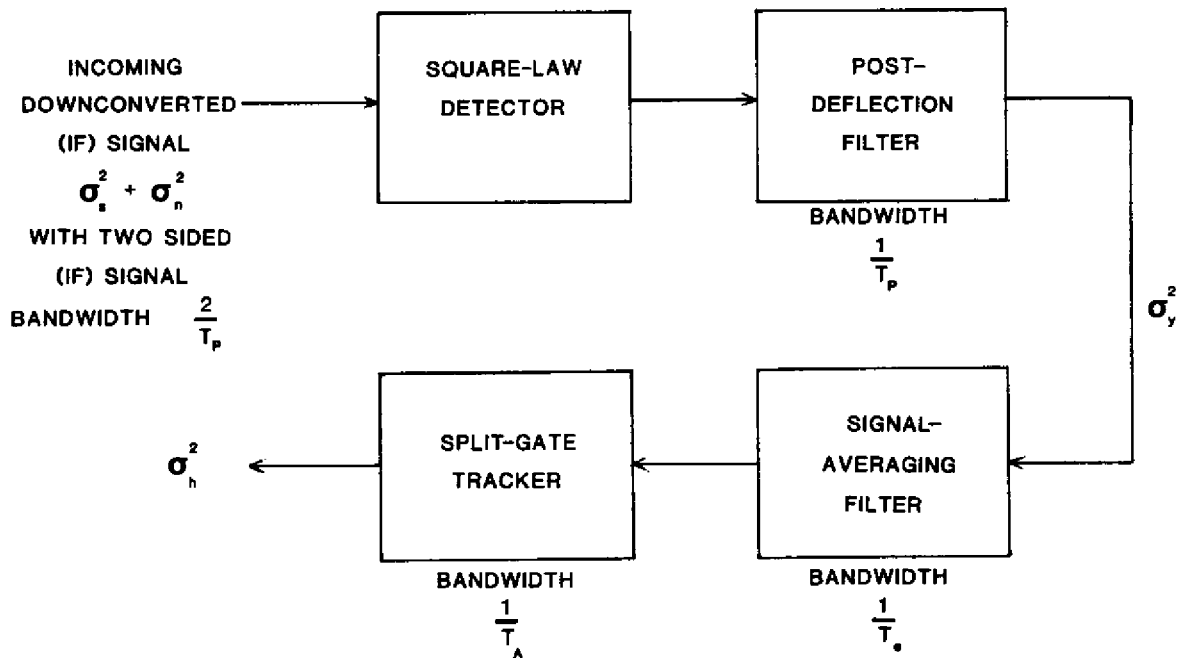


Fig. 6 — Model receiver system used to compute rms height error

The received signal, prior to detection, will comprise a zero-mean narrow-band Gaussian process. The mean square value (or the variance $\sigma_s^2(t)$) of this signal is equivalent (within a scaling factor) to the average waveform $P_r(\tau)$ discussed previously. If the additive noise variance of the receiver is denoted by σ_n^2 , the signal entering the square-law detector has the total variance equal to $\sigma_s^2 + \sigma_n^2$ and a two-sided (IF) signal bandwidth equal to $2/T_p$, where T_p (~ 3 ns) is the transmitted signal compressed pulse length. Let T_e be the time spread of $P_r(\tau)$ between the e^{-1} points. A theoretical estimate of the rms height error for a split-gate tracker can now be derived. As discussed in Davenport and Root [17], for a Gaussian input signal plus noise $\sigma_s + \sigma_n$, the square-law-detected, zonal filtered signal is exponentially distributed with the variance

$$\sigma_y^2 = a^2 \left(\sigma_s^2 + \sigma_n^2 \right)^2,$$

where a is the detection scale factor, or

$$\sigma_y = a\sigma_s^2 \left[1 + \frac{2}{\text{SNR}} + \frac{1}{\text{SNR}^2} \right]^{1/2},$$

where the signal-to-noise ratio (SNR) is defined at the peak value of σ_s^2 , i.e., $(\sigma_s^2_{\text{max}}/\sigma_n^2)$. Replacing $a\sigma_s^2$ by the range spread function $P_r(\tau)$ and considering the averaging property of the postdetection and signal-averaging filters, we obtain

$$\sigma_y = \frac{P_r(\tau)}{2} \left[\frac{T_p}{T_e} \left[1 + \frac{2}{\text{SNR}} + \frac{1}{\text{SNR}^2} \right] \right]^{1/2}, \quad (10)$$

where $(1/T_p)$ and $(1/T_e)$ are the bandwidths of the postdetection filter and the signal-averaging filter, respectively. Two filters are discussed for conceptual purposes only; in an actual system only one composite filter would be needed. Statistically independent samples spaced by T_p over the time expanse T_e have been assumed. The factor 1/2 arises from replacing the idealized zonal filter with a realizable filter [18,19].

Next we use the waveform model

$$P_r(\tau) = e^{-\left[\frac{\tau^2}{2(T_e/2)^2} \right]}, \quad (11)$$

and assume a split-gate tracker that tracks the $P_r(\tau)$ waveform at $P_r(\tau) = e^{-1/2}$. Note that the slope $\Delta\tau/\Delta P_r$ at $P_r(t) = e^{-1/2}$ is

$$\frac{\Delta\tau}{\Delta P_r} = \frac{T_e}{2e^{-(1/2)}}.$$

We next determine $\sigma_\tau = \sigma_y (\Delta\tau/\Delta P_r)$, the range uncertainty in time units, as

$$\sigma_\tau = \frac{1}{4} \left[T_p T_e \left[1 + \frac{2}{\text{SNR}} + \frac{1}{\text{SNR}^2} \right] \right]^{1/2}.$$

To convert σ_r into distance units, we use $r = (c\tau/2)$. Furthermore, considering the averaging of a number of statistically independent return waveforms over a time period T_A , we arrive at the final result for range uncertainty σ_h as

$$\sigma_h = \frac{c}{8} \left[\frac{T_p T_e}{(\text{PRF}) (T_A)} \left(1 + \frac{2}{\text{SNR}} + \frac{1}{\text{SNR}^2} \right) \right]^{1/2} \quad (12)$$

These results can be compared with the Walsh simulation results [20]. For the aircraft case with $\text{PRF} = 200$, $T_A = 0.05$ s, $T_p = 5$ ns, and $T_e = 33$ ns, Eq. (12) (for $\text{SNR} = 100$) gives $\sigma_h = 15.2$ cm. The simulation yields a value of 15 cm [20].

The previous discussion has tacitly assumed a symmetrical aperture, with equal beamwidths in both planes. The analysis is readily generalized to cover unequal along-track and cross-track beamwidths.* For the general case, σ_h can be shown to be proportional to the square root of the cross-track beamwidth divided by the along-track beamwidth. Thus minimizing σ_h requires minimizing the cross-track beamwidths and maximizing the along-track beamwidths (subject to resolution constraints).

The range noise expression depends on a number of parameters that, within engineering limitations, can be arbitrarily selected. For the PRF, however, it is desirable to use as large a value as possible. The largest value of PRF is that which ensures decorrelated returns. Larger values will reduce the effects of receiver thermal noise, but they will not reduce the effects of the inherent randomness of the return power. Since thermal noise is not the primary problem here, it does no good to use a PRF that is larger than the one for decorrelated returns.

The minimum distance necessary for the radar to travel for decorrelation may be accurately estimated from the Van Cittert-Zernike theorem [21] as modified by Walsh in Ref. 22 to account for the two-way radar path. In particular, this distance l is given by

$$l = 0.3 h\lambda/\rho, \quad (15)$$

where ρ is the radius of the illuminated spot on the surface. For the case at hand where very narrow beamwidths are considered,

$$\rho = h\theta_B/2, \quad (16)$$

so that

$$l = 0.6\lambda/\theta_B. \quad (17)$$

Using Eq. (8) to relate θ_B and the antenna aperture diameter yields

$$l = 0.408D. \quad (18)$$

*Throughout this report, we assume that only cross-track squinted beams are present; other geometries may be treated by direct analogy.

Since the PRF is given by

$$\text{PRF} = V_S/l, \tag{19}$$

therefore

$$\text{PRF} = 2.45 V_S/D,$$

where V_S is the horizontal velocity of the altimeter. Figure 7 is a plot of this relation for the present case. Substituting this result into the relationship for the range noise yields

$$\sigma_h = 0.126 c \left(\frac{h\xi T_c}{V_S f T_A} \left[1 + \frac{2}{\text{SNR}} + \frac{1}{\text{SNR}^2} \right] \right)^{1/2}. \tag{20}$$

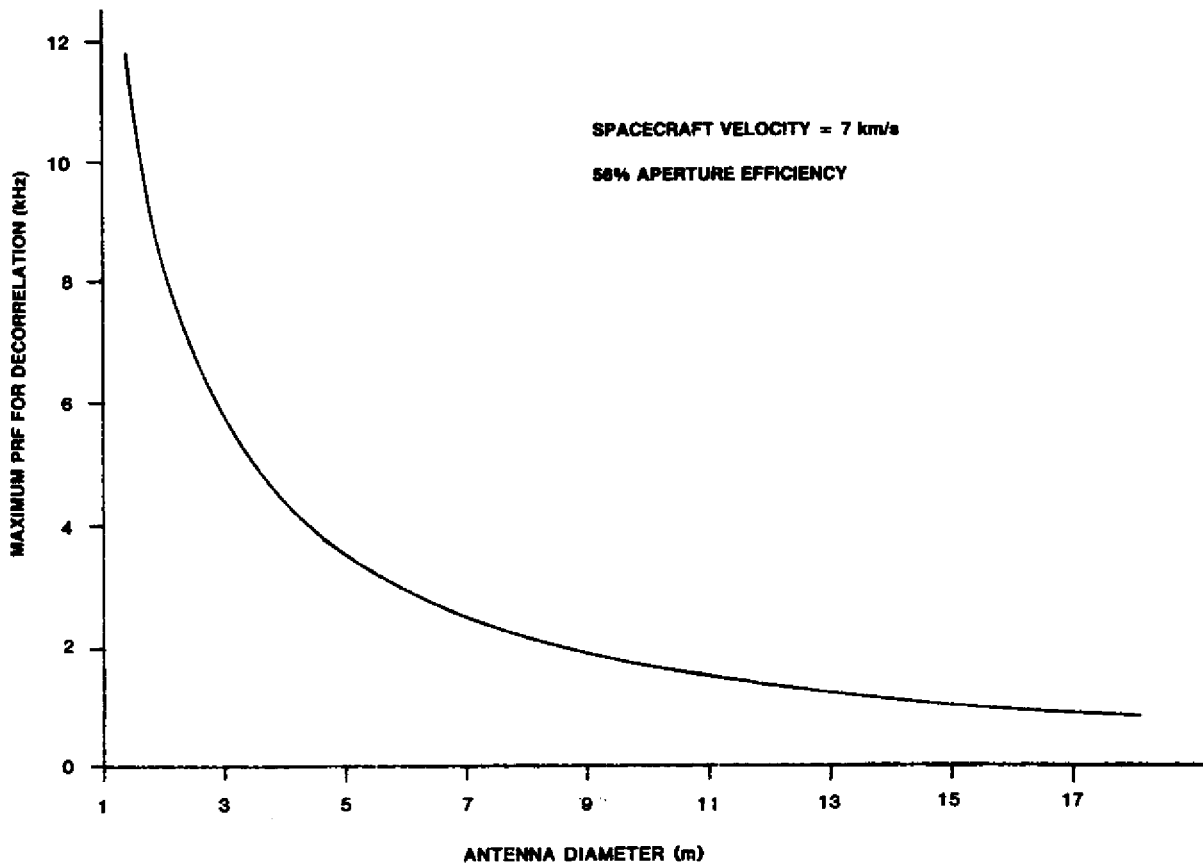


Fig. 7 — Maximum PRF for decorrelation of the returns

This result predicts higher range noise with altitude, pointing angle, and composite pulse width. Conversely, a lower range noise can be expected from increasing the altimeter's horizontal velocity, its frequency, the averaging time, and SNR. Of particular interest here is the fact that the range noise is independent of the antenna diameter for $\text{SNR} \gg 2$. This is a bit deceptive, however, since it assumes a maximum PRF. That is, since the width of the return is proportional to both the antenna diameter and the maximum PRF, these two dependencies cancel because they appear as a ratio in the expression for σ_h . Assuming that

$$T_c = 3.125 \text{ ns},$$

$$V_S = 7 \text{ km/s},$$

$$T_A = 1 \text{ s},$$

and that $\text{SNR} \gg 2$, Eq. (20) yields the following range noise values for σ_h :

$$\sigma_h = \begin{cases} 4.9 \text{ cm (13.5 GHz)} \\ 2.9 \text{ cm (36 GHz)} \end{cases} \quad (21)$$

If constraints dictate that the PRF cannot be the maximum value for a given antenna diameter (as shown in Fig. 7), range noise will increase. Figure 8 shows how the range noise increases as the PRF decreases (contracts) from its maximum value for a frequency of 13.5 GHz. Figure 9 is the same plot for 36 GHz. These curves show that a reduction in PRF from its maximum value, by a factor α , increases the range noise by $\alpha^{1/2}$.

Figures 10 and 11 are plots of SNR for 13.5 and 36 GHz, respectively, as a function of antenna diameter. In these plots, GEOSAT altimeter parameters [23] are used:

$$\eta = 32,768,$$

$$P_T = 20 \text{ W},$$

$$\sigma^0(3.58^\circ) = 10 \text{ dB},$$

Receiver NF is 5 dB,

Bandwidth is 320 MHz.

It is clear from these plots that a low SNR is not a significant problem.

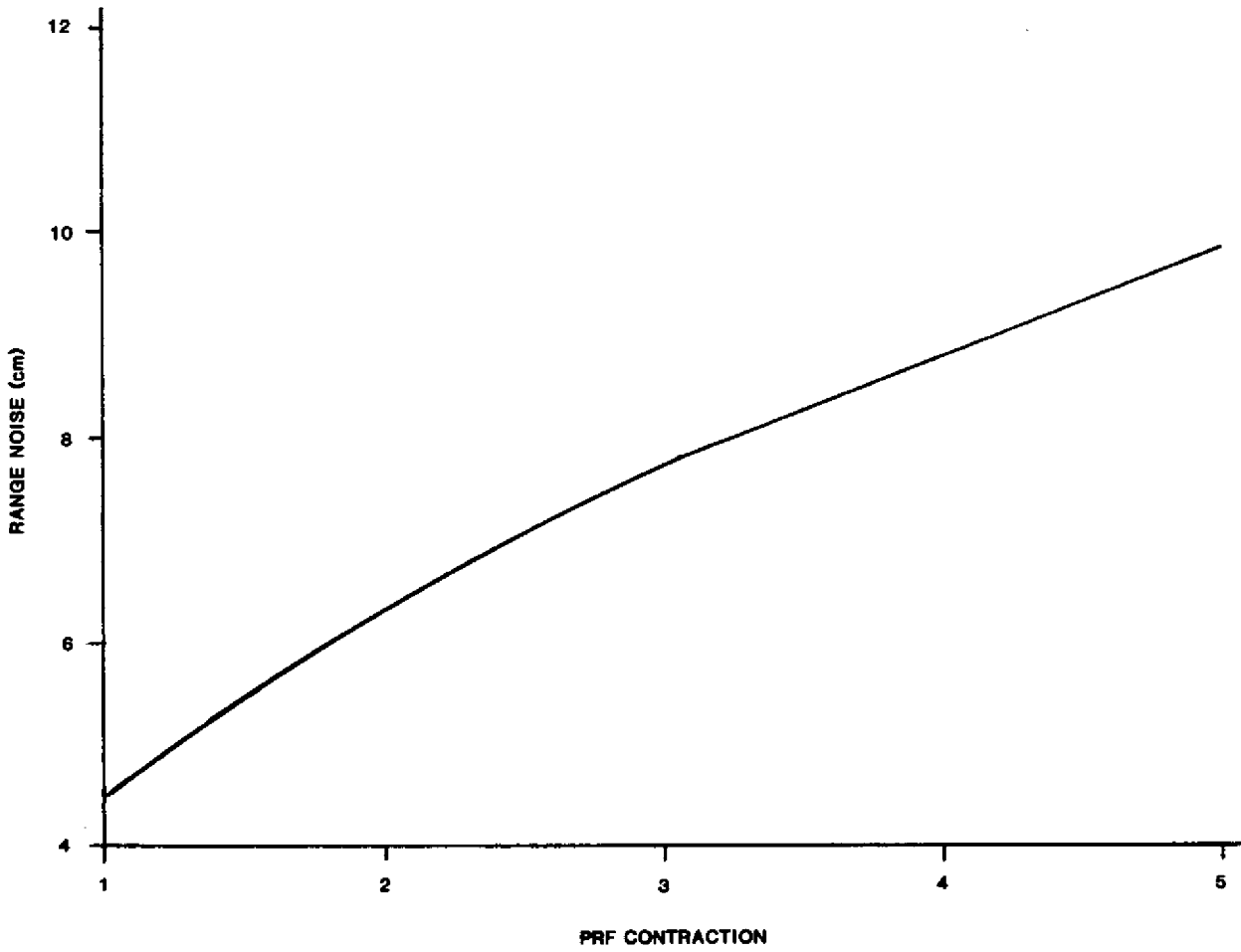


Fig. 8 — Increase in range noise with decrease or contraction of the PRF from its maximum value for 13.5 GHz

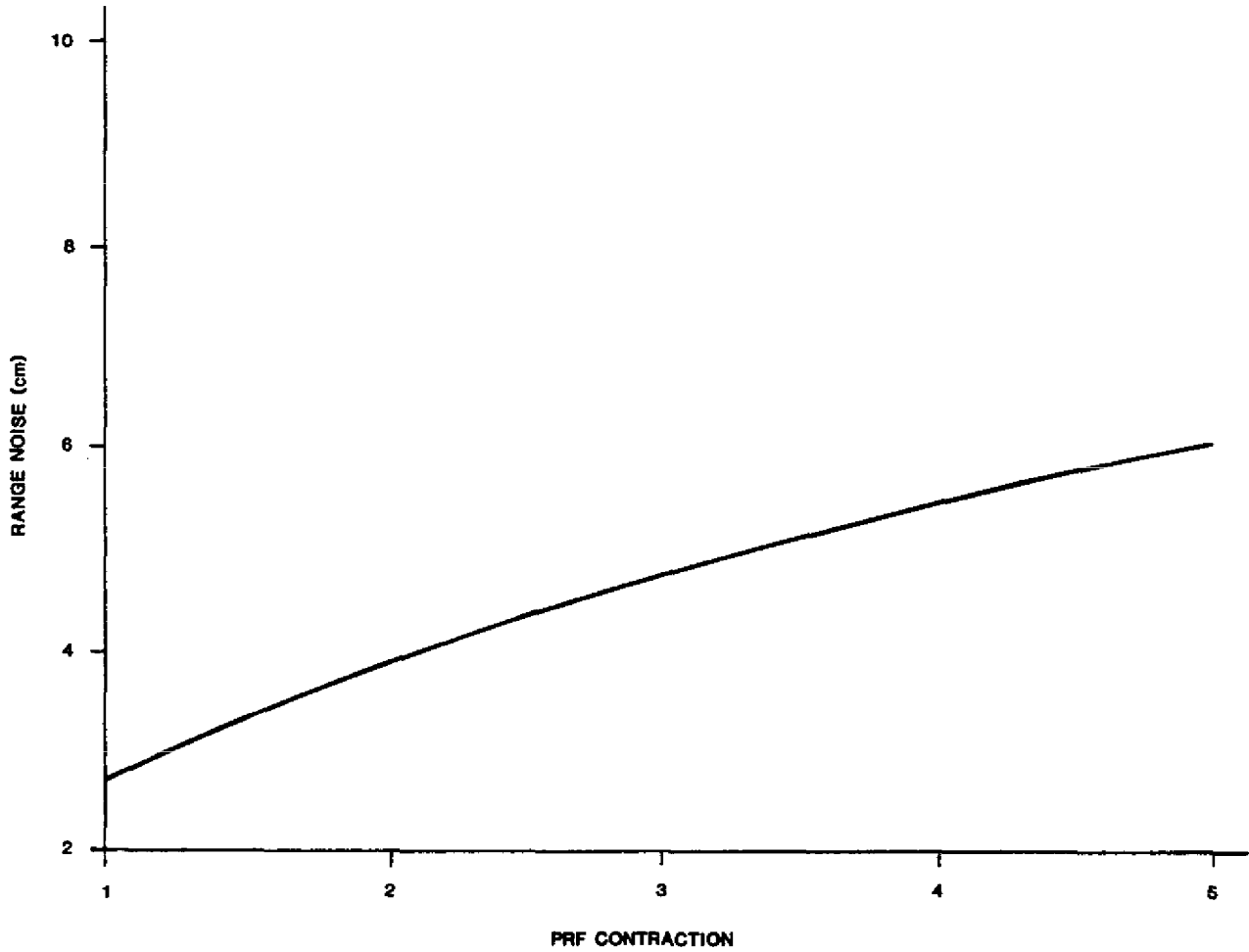


Fig. 9 — Increase in range noise with decrease or contraction of the PRF from its maximum value for 36 GHz

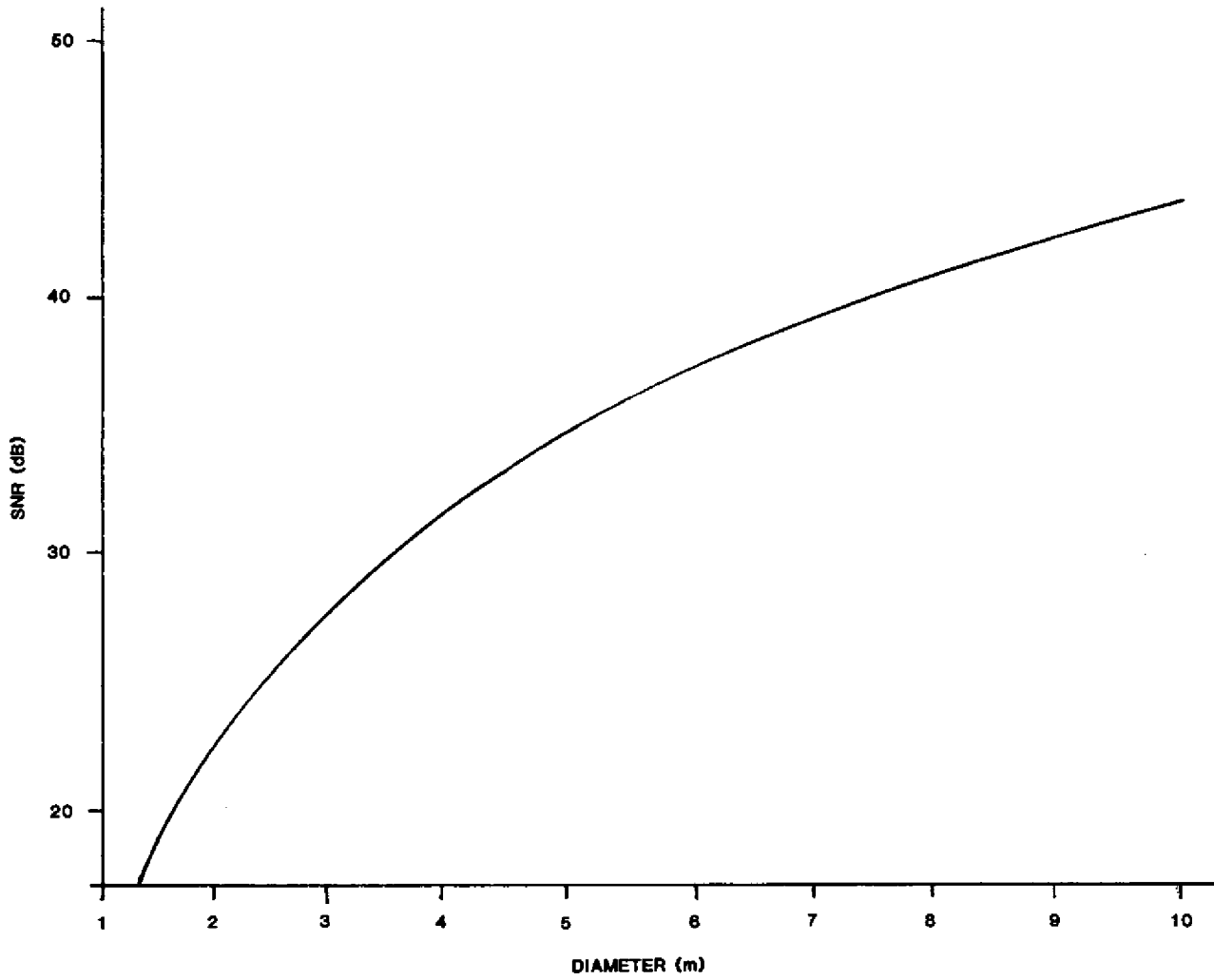


Fig. 10 — Signal-to-noise ratio for 13.5 GHz

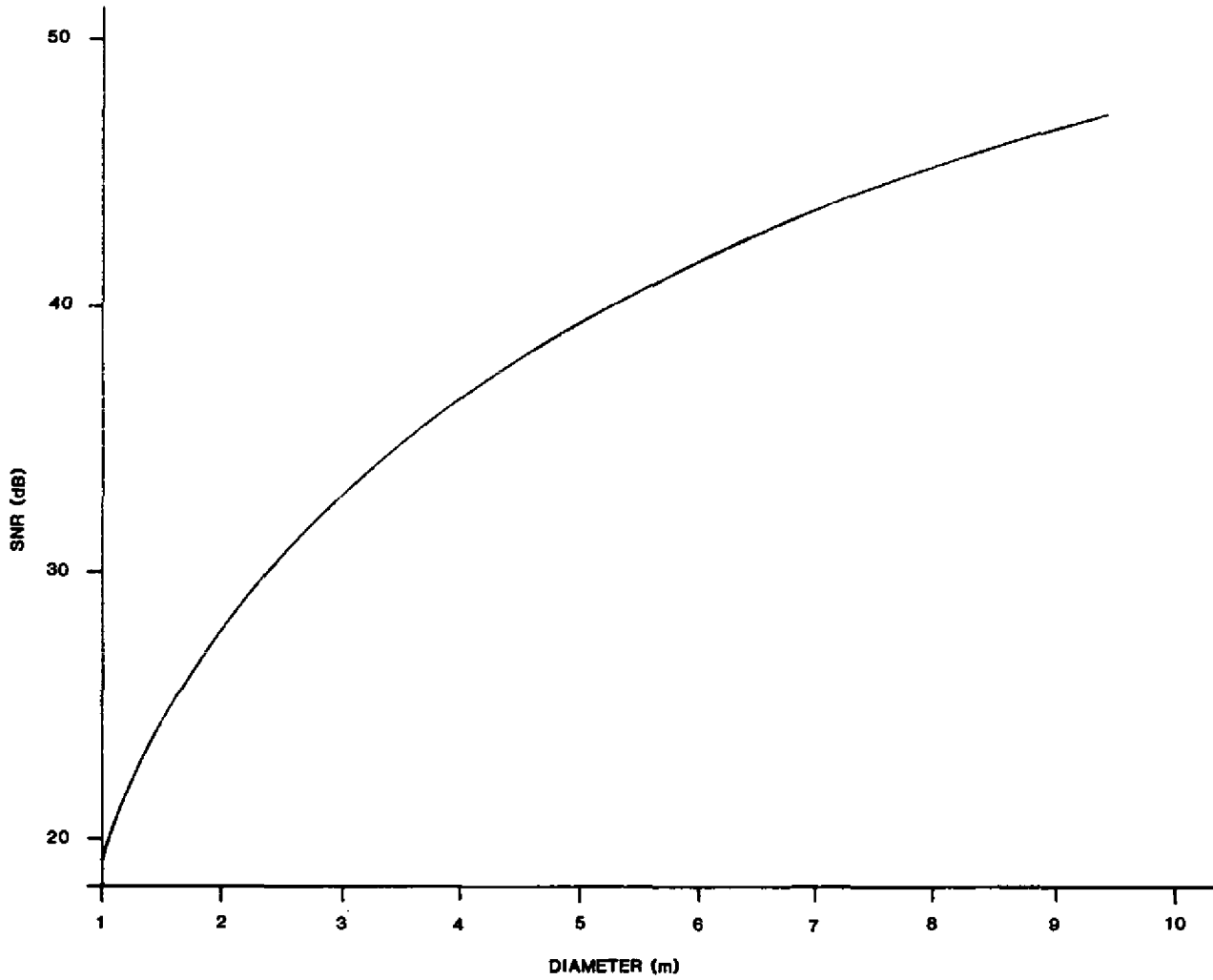


Fig. 11 — Signal-to-noise ratio for 36 GHz

We next consider the spatial resolution of this system. For mesoscale topographic mapping, some degree of correspondence should be provided between time averaging and beamwidth spatial averaging. Spatial averaging may be incorporated into the above formulation as follows. For a Gaussian antenna pattern of the form $\exp(-\theta^2/2\sigma^2)$, the two-way beamwidth in σ -units can be shown to be

$$\sigma = \frac{\theta_B}{1.664},$$

and by using $\theta_B = 1.47 \lambda/D$,

$$\sigma = 0.883 \frac{\lambda}{D}.$$

To model the overall spatial resolution, we assume that the composite spatial-averaging process results from the antenna spatial-filtering effect and averaging over the interval T_A . Assuming both averaging processes to be Gaussian functions, the convolved one-sigma width will be

$$\left[T_A^2 + \left(\frac{2\sigma r}{V_S} \right)^2 \right]^{1/2} \approx \left[T_A^2 + \left(\frac{1.776 \lambda h}{DV_S} \right)^2 \right]^{1/2},$$

where r is slant range and V_S is satellite velocity. For equal contributions from each term and $r \approx h$,

$$T_A = \frac{1.776\lambda h}{DV_S},$$

and the corresponding antenna diameter is

$$D = \frac{1.776\lambda h}{V_S T_A}.$$

Thus, based on the Nyquist criteria, the spatial resolution L (in wavelengths) is

$$L \approx 2 (2)^{1/2} V_S T_A.$$

For example, with $D = 4.5$ m, $\lambda = 0.0222$ m, $V_S = 7$ km/s, and $T_A = 1.01$ s; L is found to be 19.8 km.

One final calculation is of interest before leaving this particular system. Reference 24 has shown that front-fed parabolic reflectors can be scanned off boresight by about eight beamwidths. For larger scanning angles the antenna design becomes complex. Thus it is desirable that the pointing angle corresponding to the 50-km offset beam not exceed the eight-beamwidth criterion or

$$8\theta_B \geq 3.58^\circ \tag{22}$$

or

$$\theta_B \geq 0.45^\circ. \tag{23}$$

Using Eq. (8) gives

$$D \leq \frac{1.47 \lambda}{\theta_B},$$

or for 13.5 GHz,

$$D \leq 4.12 \text{ m.} \quad (24)$$

Figure 10 shows that the SNR for this antenna diameter is ~ 30 dB, so a low SNR is not a problem. A 4-m antenna diameter is significant from another perspective: it is near to the maximum diameter antenna that a Titan III shroud will cover.

Thus if a 4-m antenna diameter is used along with the maximum PRF, it is possible to:

- achieve a ≤ 5 -cm range noise at 13.5 GHz,
- use well-established antenna technology to generate the offset beams, and
- use an antenna that will not exceed existing launch vehicle capacity.

From these results, it is obvious that the pure multiple-beam antenna system is a viable means for achieving relatively precise off-nadir altimetry.

At 36 GHz, the propagation considerations are that ionospheric effects are negligible; however, precipitation losses are significant. A precipitation rate of 12.5 mm/h corresponds to an attenuation of ≈ 4 dB/km [25]. For a storm with a freezing level of 10 km, the two-way attenuation would be 80 dB. The corresponding figure for a rate of 2.5 mm/h is 10 dB. Thus a 36 GHz system will probably be limited to rainfall rates of < 5 mm/h for a low-power system with a solid-state transmitter. A final decision on operating frequency should be based on a detailed analysis of the percent coverage loss that this precipitation level represents.

Interferometric Approach

Figure 12 shows the interferometric approach. Two antennas are separated by a distance d in the cross-track direction and appropriately phased to shift their composite beam off-nadir by an angle ξ . Since the desired one-sided cross-track distance is 50 km, the shift angle is 3.58° . To make the footprint on the surface as small as possible, d is taken to be many wavelengths.

The derivation of the flat-surface impulse response for this configuration is somewhat involved and so it will only be highlighted here. The composite antenna pattern is a product of the pattern of the individual antennas and the so-called array factor. Since this array performs best if its boresight is shifted to the center of the desired spot on the surface, this is the case that was actually analyzed. That is, slightly better performance can be achieved with the array if its principal beam is mechanically rather than electronically shifted to the desired spot by phasing one antenna relative to the other. Another reason for doing this is to develop a general expression to deal with array pointing errors.

The resulting expression for the composite antenna pattern is a rather complicated function of geometry. To simplify the azimuthal integration in the expression for the flat-surface impulse

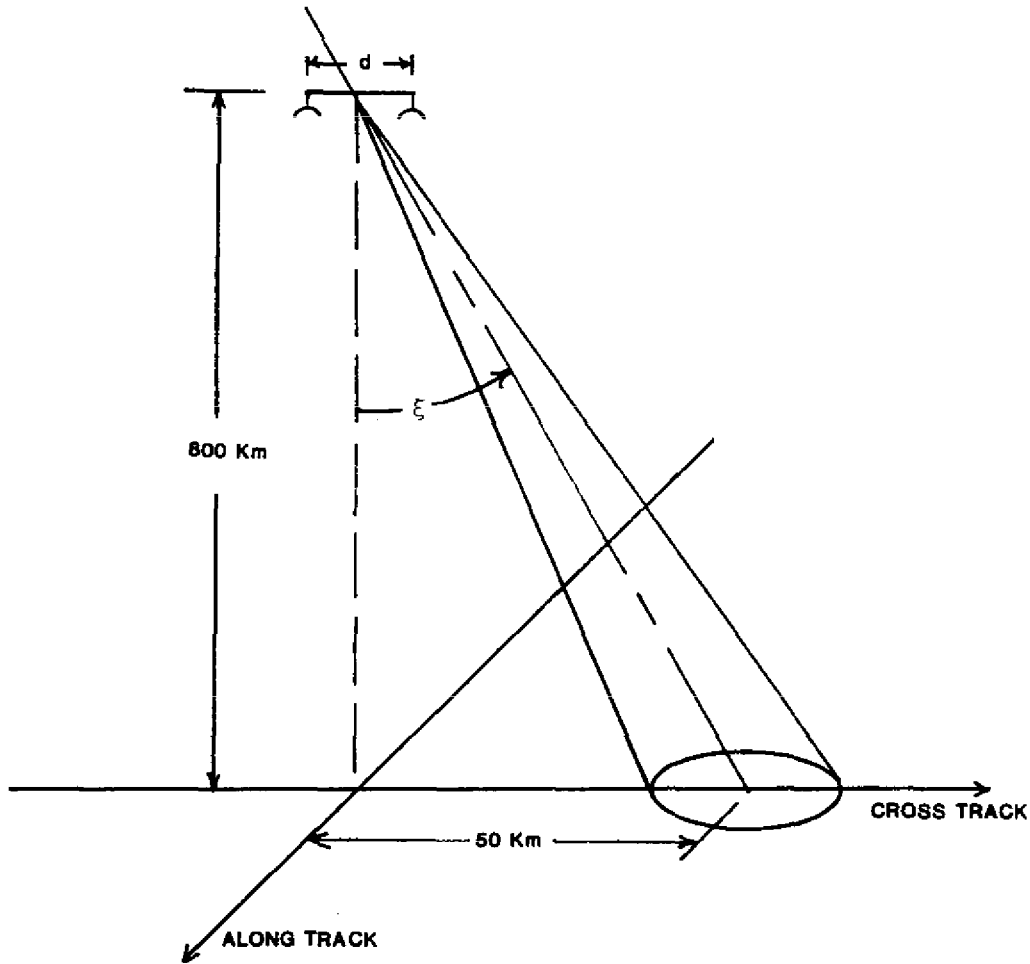


Fig. 12 — Interferometric approach to forming a narrow off-nadir beam.
The interferometer baseline is d .

response, certain large parameters are used in the system description. However, unlike the asymptotic evaluation presented in Ref. 8, the proper technique to evaluate the integral must be selected. That is, if the pattern of each antenna element is dominant, Laplace's method should be used. However, if the array factor is dominant, stationary phase should be the method of approximation. A decision can be based on the relative magnitude of $k_0 d$ compared to $(4/\gamma) \sin 2\xi$. The former represents the dominance of the array factor while the latter represents the individual antenna element. Thus, if

$$k_0 d > \frac{4}{\gamma} \sin 2\xi \gg 1, \quad (25)$$

where k_0 is the radar wavenumber ($k_0 = 2\pi/\lambda$), then the integration can be accomplished by using the stationary phase approximation. Assuming that the antenna elements comprise 56% efficient parabolic reflectors, this expression can be reduced to

$$d > 0.81 (\xi D^2 / \lambda), \quad (26)$$

where D is the diameter of the antenna element. If the equality is reversed, Laplace's method should be used. As noted in Eq. (25), either or both of these parameters must be large compared to unity, because only then can the asymptotic integration techniques be considered.

For the situation described in Ref. 12, the inequality described in Eq. (26) was indeed satisfied so that the approximate integration was accomplished with the aid of stationary phase. This led to the following approximate expression for the flat-surface impulse response when using the two-element interferometer:

$$\begin{aligned}
 P_{FS}(\tau) \approx & \frac{\eta P_T \lambda^2 \sigma^0(\psi)(c/2)}{(4\pi)^3 L_p r^3} \left\{ \left[\frac{\pi}{k_0 d |q''(0)|} \right]^{1/2} \exp \left\{ -\frac{4}{\gamma(1+\epsilon^2)} [\sin \xi - \epsilon \cos \xi]^2 \right\} \right. \\
 & \cdot \left[2 \cos \left[\frac{2k_0 d}{(1+\epsilon^2)^{1/2}} [\sin \xi - \epsilon \cos \xi] + \frac{\pi}{4} \right] \right. \\
 & \left. \left. + 8(2)^{1/2} \cos \left[\frac{k_0 d}{(1+\xi^2)^{1/2}} [\sin \xi - \epsilon \cos \xi] + \frac{\pi}{4} \right] \right] \right\} \\
 & + 6 \left[\frac{2\pi}{a(1+b/a)} \right]^{1/2} \exp \left\{ -\frac{4}{\gamma(1+\epsilon^2)} [\sin \xi - \epsilon \cos \xi]^2 \right\} \left. \right\}, \quad (27)
 \end{aligned}$$

where

$$\epsilon = (c\tau/h)^{1/2} \quad (27a)$$

$$a = \frac{4}{\gamma} \frac{\epsilon \sin 2\xi}{1+\epsilon^2}, \quad \text{and} \quad b = \frac{4}{\gamma} \frac{\epsilon^2 \sin^2 \xi}{1+\epsilon^2},$$

$$q''(0) = \frac{\epsilon}{(1+\epsilon^2)^{1/2}} \left[\cos \xi + \frac{\sin \xi - \epsilon \cos \xi}{1+\epsilon^2} \right]. \quad (27b)$$

This result can be converted to the actual average return waveform by simply multiplying Eq. (27) by the composite pulse width T_c , provided that the lobes in Eq. (27) are much wider than the composite pulse width. The angle ψ is given by

$$\tan \psi = (c\tau/h)^{1/2}. \quad (28)$$

Reference 12 provides a set of baseline parameters for a possible spaceborne application; these parameter values are

$$d = 10 \text{ m}, \quad D = 1.5 \text{ m}, \quad \text{and} \quad \lambda = 2.22 \text{ cm (13.5 GHz)}.$$

Substituting these parameters into Eq. (26) yields 5.2 for the right-hand side and 10 for the left-hand side; thus, the inequality is indeed satisfied and Eq. (27) can be used. Figure 13 is a plot of the flat-surface impulse response for the 10-m interferometer. The lobes are due primarily to the second cosine term in Eq. (27). The peak in the impulse response does not occur exactly at

$$\tan \xi = (c\tau_0/h)^{1/2}$$

because of the $\pi/4$ in the argument of the cosine terms in Eq. (27). The slight although noticeable asymmetry in the shapes of the lobes is due to the two cosine terms in Eq. (27) having different periods. The failure of the impulse response to go to zero between the peaks in the lobe structure is due to the nonzero beamwidth of the interferometer elements in the along-track direction. The slight decrease in the amplitudes of the lobes on either side of the maximum amplitude lobe is due to the effect of the 1.5-m interferometer element.

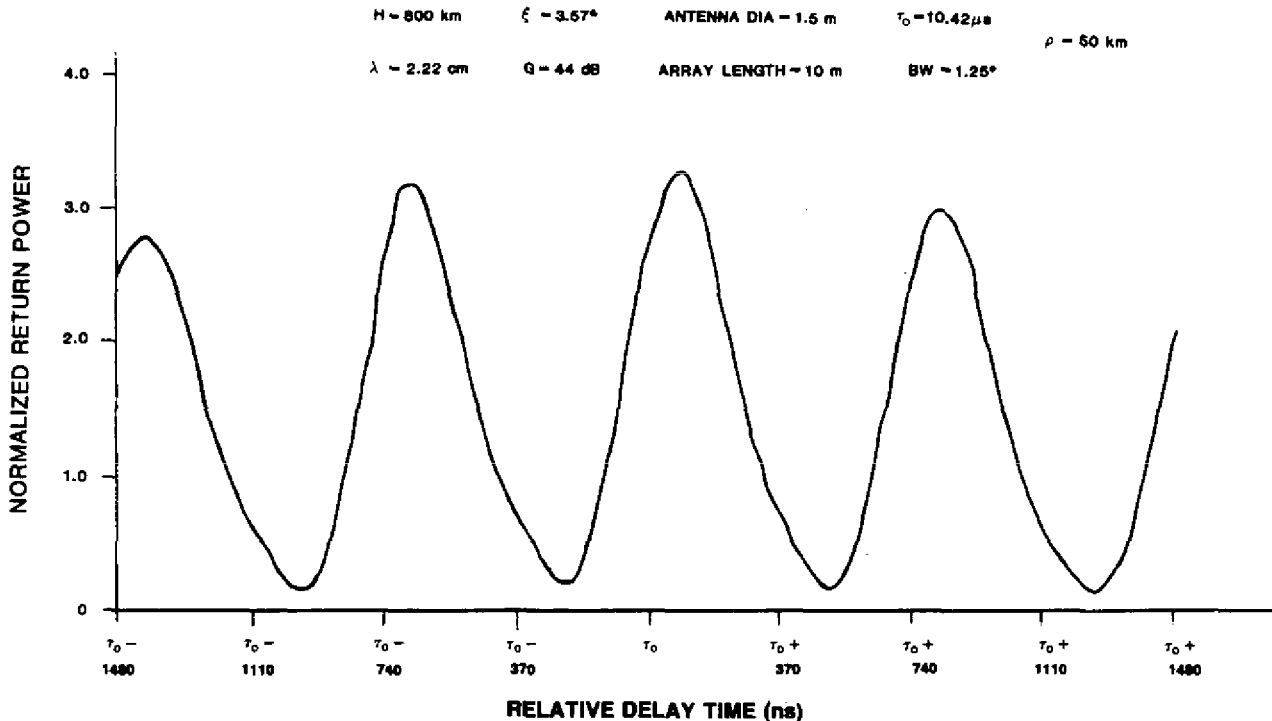


Fig. 13 — Flat-surface impulse response for the 10-m interferometer

Figure 13 clearly shows the major drawback to the interferometer approach: too many lobes are very similar in appearance. From a measurement standpoint, it would be impossible to tell a priori which lobe represents the return from the desired cell position on the earth. Designing a tracker to "look inside" a given time window would be very risky because of the possibility that the tracker would jump to the adjacent late or early lobes. This basic situation is further complicated by pointing-angle uncertainty. That is, if errors in *pointing angle and direction* are included, there may not even be a lobe which is maximum near the desired spot on the earth. For example, it may be that a local null appears at τ_0 rather than a local maximum (see Fig. 13). There is no way to compensate

for this effect unless the pointing angle and direction are known a priori. Since the pointing direction is very difficult to measure, this is a major drawback to the interferometric approach.

A possible solution to this lobe identification problem is to increase the size of the array-element antenna. This will leave the main lobe unchanged but will attenuate the adjacent lobes and, thus, make it easier to track the main lobe. Increasing the size of the array element means increasing D in Eq. (26); this will lead to a reversal of the inequality in Eq. (26) and, hence, invalidate Eq. (27). Rather than redo the derivation of Eq. (27) when the inequality in Eq. (26) is reversed, there is an easier method of estimating the effects of increasing D . By increasing D , the lobes next to the main lobe near τ_0 are decreased. The total time between the lobe just before the peak lobe and the lobe just after it is ~ 1480 ns (Fig. 13). If these lobes are to be half the peak lobe amplitude, we can use the results in Fig. 5 to estimate the diameter of the antenna element that will accomplish this. A time spread of 1380 ns requires an antenna of 5.2-m diameter at 13.5 GHz. However, this is larger than the single antenna required by the pure multiple-beam system. Thus, no real advantage to the interferometer system exists relative to the multiple-beam system.

Finally, there is yet another problem with the interferometer concept. In the actual system, the array will not be physically tilted to point to a cross track spot 50 km away from nadir. Instead, one array element will be phased relative to the other to electronically shift the beam to the desired spot. This phasing process is frequency dependent. That is, at another frequency the array will point in a different direction. Use of a 3.125-ns compressed pulse width requires a minimum bandwidth of 320 MHz that at 13.5 GHz center frequency is sufficiently large to cause a spot size shift. That is, the location of the beam spot on the surface will change over the bandwidth of the transmitted pulse.* This will have the net effect of making it even more difficult to determine exactly where on the surface the beam is located.

In summary, the interferometric approach has a major shortcoming in the number of very similar lobes it produces. Its sensitivity to pointing errors, signal bandwidth, and a 10-m phase delay path make it unsuitable for use in a spaceborne application.

Pseudo SAR

Synthetic aperture radar (SAR) is a mature technique for generating radar reflectivity images; traditionally it uses short pulses to provide high cross-track resolution (in conjunction with a flat or spherical surface assumption) and Doppler processing to provide a narrow along-track synthesized beam. The slant range (or phase) of a sequence of returns from cross-track distance x is

$$r(y) = [(h - \Delta h)^2 + x^2]^{1/2} \approx h - \Delta h + (x^2/2h).$$

For unfocused SAR, the maximum synthetic aperture length is $(h\lambda)^{1/2}$. For typical satellite altitudes at Ku-band the angular resolution is on the order of 100 m. This so-called unfocused SAR resolution may be obtained by excluding Doppler-shifted returns outside the requisite spectral range—the Doppler beam-sharpening mode. In the focused mode, higher angular resolution is achieved

*This, in effect, causes the nulls to partially fill in.

through the process of phase correcting the sequential returns prior to summation. In either case, along-track resolution is enhanced by using SAR techniques in conjunction with radar altimetry methods. Cross-track resolution is more difficult to achieve. In this case, use of short pulse length alone cannot be used to improve the cross-track resolution. For altimetry, a surface model (e.g., spherical earth) cannot be assumed since both slant range and angle-of-arrival information are needed to unambiguously determine local height. Use of conventional SAR in this context amounts to using one measurement (ranging) to determine two unknowns (slant range and angle-of-arrival). This problem has been explored by NRL and others in recent years [14,15]. These works show that an interferometric form of SAR is needed to provide both SAR resolution and altimetric data. The ambiguity problems, previously discussed in conjunction with interferometric systems also apply here. Interferometric SAR requires that two SAR systems be deployed across a reasonably long baseline. Two such phase-coherent SAR systems are not within well-developed technology; they may be considered to be future-generation sensors relative to the category under discussion. Such techniques would provide contiguous, wide-swath coverage, with higher development costs. Within the context of existing, proven technology, we return to the topic of altimetric/SAR processing to enhance along-track resolution only.

Reference 14 provides an excellent summary of altimetric/SAR capability in the along-track-only case. As discussed therein, resolution in the orthogonal coordinate must be provided by a real aperture. In the numerator of Eq. (12), T_p represents pulse width; in the denominator, PRF represents the pulse repetition frequency. Since the azimuthal resolution is restricted by the need for pulse-to-pulse decorrelation, the azimuthal (or cross-track) resolution is the only variable parameter in this case. Because this is a denominator term, for the ocean scatter with a homogeneous statistics case it should be as large as practicable within previously discussed resolution constraints. For sea ice, land, or continental ice sheet mapping, the functional behavior is far more complex. In such cases, the surface topography must be characterized. For example, with such surfaces, large-body scattering is often dominant and statistical homogeneity is grossly violated.

Pointing Angle Considerations

For pulse-length-limited, nadir-pointing altimetry, the attitude angle can be adequately estimated by examining the trailing edge of the return waveform. For beamwidth-limited, multibeam altimetry, the pointing problem is much more severe. A 5-cm height accuracy requires microradian-level attitude knowledge. References 10, 12, and 20 discuss a number of approaches to the problem, such as orbit-crossing analysis with data from geoidally quiet areas. A technique suggested by these studies is the use of a conventional GEOSAT-type altimeter to perform nadir ranging for comparison with a multibeam nadir measurement. Either along-track and cross-track Doppler measurements or a nonradar sensor would be needed to determine the Cartesian components. In any case, the pointing angle is considered to be an unresolved problem area.

CONCLUSIONS

The primary conclusion of this report is that a pure multiple-beam system has the potential for providing three beams with 50-km separation and measurements of range to a precision of better than 5 cm from an altitude of 800 km. In addition, it appears that these measurements can be achieved by using existing antenna technology. Future efforts should be directed toward experimental verification of pointing-angle determination and antenna development to provide the desired number of cross-track beams without mutual interference. Because of the near-nadir operation of this system, polarization

appears to be one way of achieving adjacent beam isolation, as originally discussed in Ref. 21. A spherical reflector with compensating feeds, such as the Arecibo concept, should also be investigated.

The interferometric approach does not appear to be as well suited to space application as originally envisioned. The multiple-lobing structure of the interferometer makes it very difficult to isolate and track any one particular lobe. If attitude errors are not properly accounted for, it becomes almost impossible to track a specific beam. If the size of the antenna elements comprising the array is increased to attenuate the unwanted lobes, these antennas must be made larger than the single antenna in the pure multiple-beam approach. In addition, the interferometer is a phased array that is sensitive to the frequency spectrum of the transmitted pulse. Furthermore, the spatial resolution is more than a factor of 2 poorer than the pure multiple-beam system considered in this report. Considering all of these and other problems leads to the conclusion that the interferometer or SAR approach is not viable for spaceborne application.

SUPPORTING AIRCRAFT EXPERIMENTATION

A number of questions regarding the viability of the multibeam altimetry can be resolved in the laboratory and on airborne platforms. An airborne system is essential for obtaining the much-needed data from the open ocean to validate the theoretical computations and predictions and to develop and evaluate real-time measurements and off-line data-processing algorithms.

Two multibeam altimeter systems for airborne platforms are being developed, a 13.5 GHz system at the Naval Research Laboratory and a 36 GHz system at NASA/Wallops. Currently a Memorandum of Understanding exists between the two laboratories to share resources and perform experiments that will complement each other's research effort.

The multibeam system under development at NRL has the following characteristics:

Number of beams	2 to 5
Frequency	13.5 GHz
Transmitted peak power	1 kW
Bandwidth	700 MHz
Pulse width	3 to 10 ns
PRF	0.1 to 10 kHz
Maximum off-nadir pointing	12.5°
Beamwidth	<2°
Nominal operating altitude	3000 m

The planned areas of experimentation at NRL are:

- Verify basic scattering physics relative to mean value waveform shapes and fluctuation statistics
- Measure the sensitivity of waveform to sea state changes as pointing angle is varied from 0° to 12.5°
- Acquire off-nadir waveform data by using a nadir beam tracker to control the off-nadir waveform samplers; use these off-nadir data to evaluate various range tracking schemes

- Determine adjacent beam coupling
- Perform pointing angle determination studies
- Study off-nadir beam gain normalization problems
- Observe off-nadir wind speed (σ^0)
- Gain actual experience with the interferometer ambiguity problem

ACKNOWLEDGMENTS

The authors thank Dr. Vincent Noble for his encouragement and support. Our appreciation also goes to Marie Sprangler and Linda Ridgely for typing the manuscript and to Joseph Shuhly for general editing. This work is supported by SPAWAR SPACETASK 141-D-NRL-C-9 (X1596).

REFERENCES

1. RADM J.R. Seesholtz, Oceanographer of the Navy, CNO ltr Ser. 0060/6U449045, 14 Oct. 1986.
2. Proceedings of the Ocean Prediction Workshop 1986, The Institute of Naval Oceanography/NSTL, MS 39529.
3. Harley E. Hurlburt, "The Potential for Ocean Prediction and the Role of Altimeter Data," *Marine Geodesy* 8(1-4), 1984.
4. Potential Environmental Sensor Enhancements for the N-ROSS Series Satellites, NORDA R/S 001561-85, June 1985. A.E. Pressman, Editor.
5. J.L. Mitchell, Z.H. Hallock, J.D. Thompson, "REX and GEOSAT: Progress in the First Year," *Johns Hopkins Tech. Digest* 8(2), Apr-Jun 1987.
6. S. Itzikowitz, M.J. Jacobson, and W.L. Siegmann, "Modeling of Long-range Acoustic Transmissions Through Cyclonic and Anticyclonic Eddies," *J. Acoust. Soc. Am.* 73, 1556-1566 (1983).
7. G.S. Brown, "The Average Impulse Response of a Rough Surface and Its Applications," *IEEE Trans. Antennas Propag.* AP-25, 67-74, (1977).
8. D.J. Kirchner, G.S. Brown, and B.A. Davis, "Research on Multibeam Altimetry and Electromagnetic Bias," Final Report on NASA Grant NAG5-636, prepared by Virginia Polytechnic Institute and State University, Blacksburg, VA, April 1988.
9. G.S. Brown, "Multiple Beam Radar Altimetry for Oceanographic and Terrain Remote Sensing," Concept Memorandum, Applied Science Associates, Inc., Apex, NC, May 1976.

10. G.B. Bush, E.B. Dodson, R. Matyskiela, E. Walsh, and C.C. Kilgus, "An Analysis and Simulation of the Multibeam Altimeter," JHU Technical Memorandum, Mar. 1980.
11. J.T. McGoogan and E.J. Walsh, "Real-time Determination of Geophysical Parameters from a Multibeam Altimeter," AIAA/NASA Conference on "Smart" Sensors, Hampton, VA, Nov. 1978.
12. J.L. MacArthur and C.C. Kilgus, "Multibeam Altimeter Conceptual Design Package," transmitted under cover letter from T. Wyhatt to V. Noble (NRL), July 1985.
13. E. Brookner (ed.), *Radar Technology* (Artech House, Norwood, MA, 1977).
14. H.D. Griffiths, "Synthetic Aperture Processing for Full-deramp Radar Altimeters," *Electronics Letters* 24(7), 371-373 (1988).
15. L.S. Miller, "Interferometer Radar," final report on NRL Contract N00173-78-C-0138 by Applied Science Assoc. Inc., Apex, NC, July 1981.
16. S. Silver (ed.), *Microwave Antenna Theory and Design* (McGraw-Hill Book Co., New York, 1949) p. 195.
17. W. Davenport and W. Root., *Random Signals and Noise*, (McGraw-Hill Book Co., New York, 1958) pp. 253-259.
18. B. Steenson, and N. Sterling, "The Amplitude Distribution and False Alarm Rate of Filtered Noise," *Proc. IEEE*, 42-55 (1965).
19. L.S. Miller and G.S. Hayne, "Characteristics of Ocean Reflected Short Radar Pulses with Application to Altimetry and Surface Roughness Determination," in *Sea Surface Topography from Space*, (J. R. Apel, ed.) NOAA Tech. Rep. ERL 228-AOML, May 1972, vol. 1, pp. 121-132.
20. E.J. Walsh, "Off-Nadir Return Waveform Variation and Tracker Simulation," NASA Wallops Flight Facility Tech. Memo, July 1987.
21. M. Born and E. Wolf, *Principles of Optics*, MacMillian Co., 1964, pp. 508-512.
22. C.L. Parsons and E.J. Walsh, "Off-Nadir Radar Altimetry," *IEEE Trans. Geoscience Remote Sensing* 27(2) (1989).
23. Special Edition, "The Navy GEOSAT Mission," *APL Technical Digest*, 8, 169-266 (1987).
24. W.C. Wong "On the Equivalent Parabola Technique to Predict the Performance Characteristics of a Cassegrainian System with an Offset Feed," *IEEE Trans. Antennas Propag.* AP-21 335-339 (1973).
25. M.I. Skolnik (ed.) *Radar Handbook*, (McGraw-Hill Book Co., New York, 1970) pp. 23-24,28.